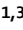





OPEN

Contribution of local and surrounding anthropogenic emissions to a particulate matter pollution episode in Zhengzhou, Henan, China

Yaobin Wang^{1,3}, Feng Wang^{1,3}, Ruiqi Min³, Genxin Song³, Hongquan Song^{1,2}, Shiyang Zhai^{1,3}, Haoming Xia¹, Haopeng Zhang^{1,3} & Xutong Ru^{1,3}

In this study, we simulated the spatial and temporal processes of a particulate matter (PM) pollution episode from December 10–29, 2019, in Zhengzhou, the provincial capital of Henan, China, which has a large population and severe PM pollution. As winter is the high incidence period of particulate pollution, winter statistical data were selected from the pollutant observation stations in the study area. During this period, the highest concentrations of PM_{2.5} (atmospheric PM with a diameter of less than 2.5 µm) and PM₁₀ (atmospheric PM with a diameter of less than 10 µm) peaked at 283 µg m⁻³ and 316 µg m⁻³, respectively. The contribution rates of local and surrounding regional emissions within Henan (emissions from the regions to the south, northwest, and northeast of Zhengzhou) to PM concentrations in Zhengzhou were quantitatively analyzed based on the regional Weather Research and Forecasting model coupled with Chemistry (WRF/Chem). Model evaluation showed that the WRF/Chem can accurately simulate the spatial and temporal variations in the PM concentrations in Zhengzhou. We found that the anthropogenic emissions south of Zhengzhou were the main causes of high PM concentrations during the studied episode, with contribution rates of 14.39% and 16.34% to PM_{2.5} and PM₁₀, respectively. The contributions of anthropogenic emissions from Zhengzhou to the PM_{2.5} and PM₁₀ concentrations in Zhengzhou were 7.94% and 7.29%, respectively. The contributions of anthropogenic emissions from the area northeast of Zhengzhou to the PM_{2.5} and PM₁₀ concentrations in Zhengzhou were 7.42% and 7.18%, respectively. These two areas had similar contributions to PM pollution in Zhengzhou. The area northeast of Zhengzhou had the lowest contributions to the PM_{2.5} and PM₁₀ concentrations in Zhengzhou (5.96% and 5.40%, respectively).

Particulate matter (PM) in the ambient air is a mixture of solid particles and liquid droplets, which are mainly generated from natural sources (e.g., dust events, wildfires, volcanic eruptions, and sea spray), anthropogenic emissions (e.g., vehicular emissions, industrial emissions, power plants, and household emissions), and atmospheric transformation^{1–4}. PM includes inhalable particles with diameters that are generally less than 10 µm (PM₁₀) and fine particles with diameters that are generally smaller than 2.5 µm (PM_{2.5})⁵. Inhalable particles pose great risks to human health by lodging deep into the lungs, and some may even enter the human bloodstream^{6–9}. Fine particles can also reduce visibility, change the radiative balance, and affect the diversity of ecosystems^{10–15}. China has experienced severe air pollution characterized by high concentrations of particulate matter due to rapid economic development, urbanization, and industrialization over the past several decades, especially in highly populated and developed urban regions such as the Pearl River Delta (PRD), the Yangtze River Delta (YRD), and the Beijing-Tianjin-Hebei (BTH)^{16–20}.

¹Key Laboratory of Geospatial Technology for the Middle and Lower Yellow River Regions, Ministry of Education, Henan University, Kaifeng 475004, Henan, China. ²Henan Key Laboratory of Integrated Air Pollution Control and Ecological Security, Henan University, Kaifeng 475004, Henan, China. ³Institute of Urban Big Data, College of Geography and Environmental Science, Henan University, Kaifeng 475004, Henan, China. ✉email: gxsong@henu.edu.cn; hqsong@henu.edu.cn

Source apportionment that quantifies the contribution of sources to air pollutants is the basis for formulating air pollution control strategies and includes two methods of receptor models and air quality models²¹. Receptor models such as chemical mass balance (CMB)^{22,23} and positive matrix factorization (PMF)^{23–25} can estimate the relationship between receptors and sources on the basis of measurements. Numerous studies have been conducted to quantify the contribution of emission sources to PM in Chinese cities, especially over the regions of the PRD, YRD and BTH^{26–28}. However, receptor models still show great uncertainty because they often adopt a fixed profile for secondary sources²¹ and cannot distinguish whether the contribution of local or regional transport plays a leading role in formulating PM control strategies²⁹. In addition, the source apportionment results of receptor models have had limited spatial coverage due to the limited samples and large spatial span of potential sources and receptor sites³⁰.

Air quality models use mathematical and numerical techniques to simulate the physical and chemical processes that affect the dispersion, formation, transport, and deposition of air pollutants in the atmosphere. They have been recognized as a useful tool for air pollution controls due to their ability and large spatial coverage to quantify the transport impacts of regional air pollutants^{31–35}. Many studies have been conducted to quantify the contributions of regional sources to PM over severely polluted regions of China, such as BTH³⁶, PRD^{37–39}, YRD⁴⁰, North China Plain (NCP)⁴¹, and western China^{42,43}, by using air quality models, such as the Weather Research and Forecasting model coupled with Chemistry (WRF/Chem)⁴⁴ and the Community Multiscale Air Quality model (CMAQ)⁴⁵. They mostly used air quality models to simulate the concentration of particulate matter in the study area at a time when the region is prone to heavy air pollution (generally, the simulation time is half a month to one month). Therefore, they can evaluate the model performance by comparing the model results to the monitoring data and analyzing the pollutant variability and influencing meteorological factors in the study region^{32,33}. Chen et al. found that the ambient PM_{2.5} at Lingcheng (a district of Dezhou city in Shandong Province) was affected not only by emissions from local and circumjacent areas; emissions resulting from regional and long-range transport also needed to be considered. Chang et al. found that in July, the local contributions to PM_{2.5} pollution in Beijing were only 33%, with contributions of approximately 3.6–5.3 µg m⁻³ coming from Shandong Province and Henan Province. These findings provide a basis for the design and implementation of emission control strategies to improve the regional air quality of China.

Most of the previous studies on PM source apportionment in China using air quality models mainly focused on populated and economically developed regions, such as the PRD, YRD, and BTH. Henan is the most populous province in central China and has become one of the most severely PM-polluted regions of China³³. Zhengzhou, the capital of Henan Province, is located in the air pollutant transport route from the severely polluted region of BTH and suffers severe particulate matter pollution problems, especially in winter⁴⁶. Urban PM is mainly generated from sources such as vehicle emissions, road/soil dust, biomass burning, agricultural emissions, and regional transport aerosols; however, studies have not yet quantified the contribution of each source or explained the formation mechanism of PM_{2.5}⁴⁷. In recent years, several studies have quantified the source apportionment of PM_{2.5} in Zhengzhou by using receptor models^{46,48–50}. Nevertheless, the contributions of local emissions and regional transport to PM in Zhengzhou and Henan Province remain unclear, which makes it difficult to understand the source and formation mechanism of PM in this region.

Winter is the high incidence period of particulate pollution, hence, the simulation study period was selected according to the statistical data of pollutant observation stations in the study area. A severe PM pollution event in the winter of 2019 in Zhengzhou gave us the opportunity to study the local and regional transport of PM pollution in Zhengzhou as a first step toward understanding where the pollution in Zhengzhou originates. We adopted the WRF/Chem model to quantify the contributions of local and surrounding anthropogenic emissions within Henan Province to particulate matter concentrations during a severe PM pollution episode from December 10–29, 2019, in Zhengzhou. The contribution rates of local emissions and emissions in areas northeast (Xinxiang and Kaifeng), northwest (Luoyang and Jiaozuo), and south (Pingdingshan and Xuchang) to Zhengzhou were analyzed during this pollution episode. The findings of this study may provide data and model references for subsequent relevant research and the scientific and rational guidance of local PM pollution control policy-making.

Materials and methods

WRF/Chem model. WRF/Chem is a collaboration between several organizations, principally the National Oceanic and Atmospheric Administration (NOAA), National Center for Atmospheric Research (NCAR), Pacific Northwest National Laboratory (PNNL) and National Aeronautics and Space Administration (NASA), as well as many other institutes^{51,52}. The model is a next-generation mesoscale numerical weather prediction system designed to serve both operational forecasting and atmospheric research needs. With the temporal and spatial resolutions completely connected online with a meteorological module and chemical module, all the emissions, transport, mixing, and chemical transformations of trace gases and aerosols can be modeled simultaneously with the meteorological module⁵³. Grell et al.⁵⁴ described WRF/Chem in detail, and Tie et al.⁵⁵ modified its chemical scheme. More detailed descriptions of WRF/Chem can be found in previous studies, such as Grell et al.⁵⁴. The performance of the WRF/Chem model for air pollutant concentration simulation has been verified by many studies^{31,51,52,56}. The map of the WRF/Chem simulation results is created in NCAR Command Language (NCL, <https://www.ncl.ucar.edu/>).

Hysplit-4 model. The HYSPLIT-4 model was jointly developed by the Air Resources Laboratory of the National Oceanic and Atmospheric Administration (NOAA) and the Australian Bureau of meteorology. It can be used to calculate a simple air mass trajectory and simulate complex diffusion and sedimentation, such as sand dust, PM_{2.5}, fire, volcanic ash, etc. At present, it has been widely used in the calculation of backward trajectories

and the study of pollutant transport and diffusion⁵⁷. It can qualitatively understand the potential sources of pollutants by simulating the area through which the air mass passes before reaching the area of concern.

Model settings. In this study, a triple-nested region was implemented from China to Zhengzhou (Fig. 1). Domain 1 comprised a large area of China with a horizontal resolution of 27 km and mainly provided initial and boundary conditions for the inner grids. Domain 2 included central China and North China at a horizontal resolution of 9 km, and Domain 3 spanned Zhengzhou and its surrounding areas at a horizontal resolution of 3 km. A spin-up period of 168 h was used to minimize the influence of the initial conditions. The vertical structure of the model includes 34 layers covering the whole troposphere. The chemical conditions at the lateral boundaries were constrained by a global chemical transport model. The Lin et al. microphysics scheme⁵⁸, the Mellor-Yamada-Janjic (Eta) turbulent kinetic energy (TKE) scheme, and the Noah land surface model were used in this study. The atmospheric shortwave and longwave radiation fluxes were computed using the (old) Goddard shortwave scheme and Goddard scheme, respectively. The Carbon Bond Mechanism version Z (CBMZ) model was used as the gas-phase chemistry scheme⁵⁹. The Madronich fast tropospheric-ultraviolet visible (F-TUV) photolysis scheme was used for the particulate matter simulations. Table 1 shows the WRF/Chem configurations of the physical and chemical options.

Datasets and experimental configuration. The model was initialized with the initial meteorological and boundary conditions using the National Center for Environmental Prediction (NCEP) Final Analysis (FNL) reanalysis datasets with a spatial resolution of $1^\circ \times 1^\circ$ and a 6-h temporal resolution. Community Atmosphere Model with chemistry (CAM-CHEM) data were adopted as the chemical conditions at the lateral boundaries. Meteorological and chemical observational datasets comprising historical air quality data recorded in China

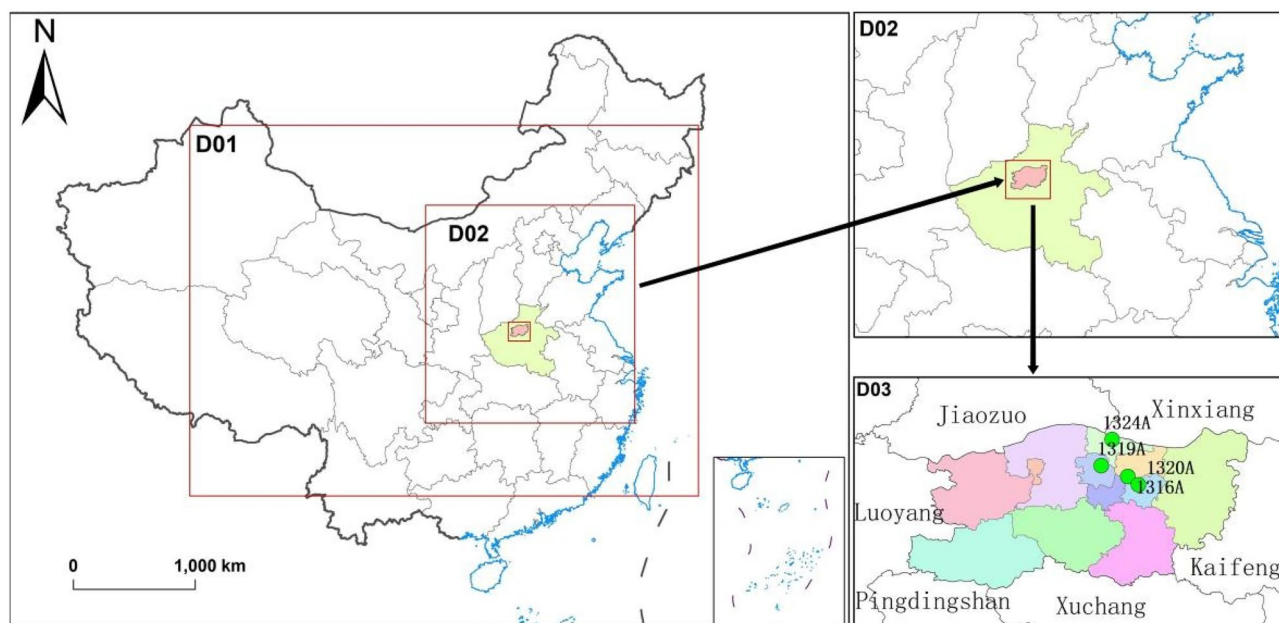


Figure 1. Simulation domain configuration of the WRF/Chem model.

Type	Scheme	Domain 1	Domain 2	Domain 3
Physics	Microphysics	Lin et al	Lin et al	Lin et al
	Planetary boundary layer	MYJ	MYJ	MYJ
	Cumulus parameterization	GF	GF	GF
	Longwave radiation	New Goddard	New Goddard	New Goddard
	Shortwave radiation	Goddard	Goddard	Goddard
	Land-surface	Noah	Noah	Noah
Chemistry	Gas phase chemistry	CBM-Z	CBM-Z	CBM-Z
	Aerosol	MOSAIC	MOSAIC	MOSAIC
	Photolysis	Madronich F-TUV	Madronich F-TUV	Madronich F-TUV
	Aerosol feedback	Open	Open	Open

Table 1. Physics and chemistry options used for the simulation cases.

were used for the model evaluation. The evaluated meteorological variables included the temperature at 2 m, wind speed at 10 m, and wind direction at 10 m. The evaluated chemical species included hourly PM_{2.5} concentrations and hourly PM₁₀ concentrations. For the emission inventory, we used the Multiresolution Emission Inventory for China (MEIC) data, which provided all anthropogenic emissions of eight species, including sulfur dioxide (SO₂), nitrogen oxides (NO_x), carbon monoxide (CO), nonmethane volatile organic compounds (NMVOCs), ammonia (NH₃), organic carbon (OC), respirable particulate matter (PM₁₀), and fine particulate matter (PM_{2.5}), in China; these emissions species have been divided into five source departments: electric power, industry, civil use, transportation, and agriculture. This inventory has been widely used to address regional air quality modeling⁶⁰.

The simulation period of this study covered from December 10 to 29 in 2019 and removed the 7-day model spin-up time. This study used December 17–29 for analysis. Meteorological conditions can be affected by aerosols, as indicated by Yang et al.⁶¹, therefore, the model was initialized with the same initial meteorological and boundary conditions. The model uses the same FNL data to provide initial meteorological and boundary conditions in different simulation schemes to ensure the consistency of meteorological conditions in different simulation experiments. Simulations were run separately for the five different emission-control scenarios, namely, S1, S2, S3, S4, and S5 (Table 2). The S1 scenario corresponded to the situation in which the emissions of pollution sources were considered in all regions in the study area (Zhengzhou and six cities around Zhengzhou). S2, S3, S4, and S5 corresponded to pollution control scenarios in Zhengzhou and in the areas to the northeast of Zhengzhou (Xinxiang and Kaifeng), to the northwest of Zhengzhou (Luoyang and Jiaozuo), and to the south of Zhengzhou (Pingdingshan and Xuchang), respectively. The contribution of each region was calculated by using the following formulas:

$$C_x = C - C_z \quad (1)$$

$$P_x = \frac{C_x}{C} \times 100\% \quad (2)$$

where C represents the benchmark PM concentration; C_z is the PM concentration when the emissions of the region are set to zero; C_x represents the difference in PM concentrations between emissions that were turned on and off in the region; and P_x represents the contribution of emissions from the region. Similar methods have been used in other air-quality-modeling studies^{62,63}.

Results

Model performance evaluation. To evaluate the performance of the WRF/Chem model, we compared the simulated and measured PM_{2.5} and PM₁₀ concentrations (Figs. 2 and 3). The temporal trends of the simulated PM_{2.5} and PM₁₀ concentrations were consistent with the observations at all 4 observation sites. In addition, these figures suggested the existence of temporal discrepancies between the peak simulated concentrations and peak observed concentrations. We can see that the WRF/Chem model can accurately simulate PM concentrations in Zhengzhou.

The validation results of the chemical and meteorological fields are shown in Table 3. The correlation coefficients (R) were 0.67, 0.55, 0.67, 0.38, 0.85 and 0.6 for the PM_{2.5} concentration, PM₁₀ concentration, wind direction (DIR), wind speed (SPD), temperature (TMP) and precipitation (PRE), respectively. The highest R and lowest mean bias (MB) values were obtained for the simulated surface temperature. For the wind field simulation, the simulation deviation of the wind speed was - 0.78 m s⁻¹, NMB was - 18%, and the correlation coefficient was approximately 0.4. The simulation deviation of the wind direction was - 6.15°, NMB was - 4%, and the correlation coefficient was 0.67. In general, the simulated wind speed was underestimated to a certain extent, which may have been caused by the wind field assimilation parameters of the four dimensional data assimilation (FDDA) used in this study for the WRF/Chem model. However, this was a slightly better estimation than those in other similar studies^{52,64,65}. Overall, regardless of which site was selected, the simulated results agreed well with observations of atmospheric pollutants during the period investigated. The intercomparisons between simulated and observed concentrations indicated that WRF/Chem notably reproduced the observed time series of PM_{2.5} and PM₁₀. However, the model tended to overestimate the concentrations of PM_{2.5} and PM₁₀.

Spatial and temporal variations in PM concentrations. The spatial distribution of the mean PM_{2.5} concentrations was basically consistent with that of the mean PM₁₀ concentrations (Fig. 4). However, the PM_{2.5} concentrations were approximately 10–20 μg m⁻³ lower than the PM₁₀ concentrations at the same location. The

Code	Emission-control scenarios
S1	Considering all pollution sources in the study area (Zhengzhou and six surrounding cities)
S2	Controlling the pollution sources in Zhengzhou
S3	Controlling the pollution sources in the northeast of Zhengzhou (Xinxiang and Kaifeng)
S4	Controlling the pollution sources in the northwest of Zhengzhou (Luoyang and Jiaozuo)
S5	Controlling the pollution sources in the south of Zhengzhou (Pingdingshan and Xuchang)

Table 2. Description of simulation scenarios.

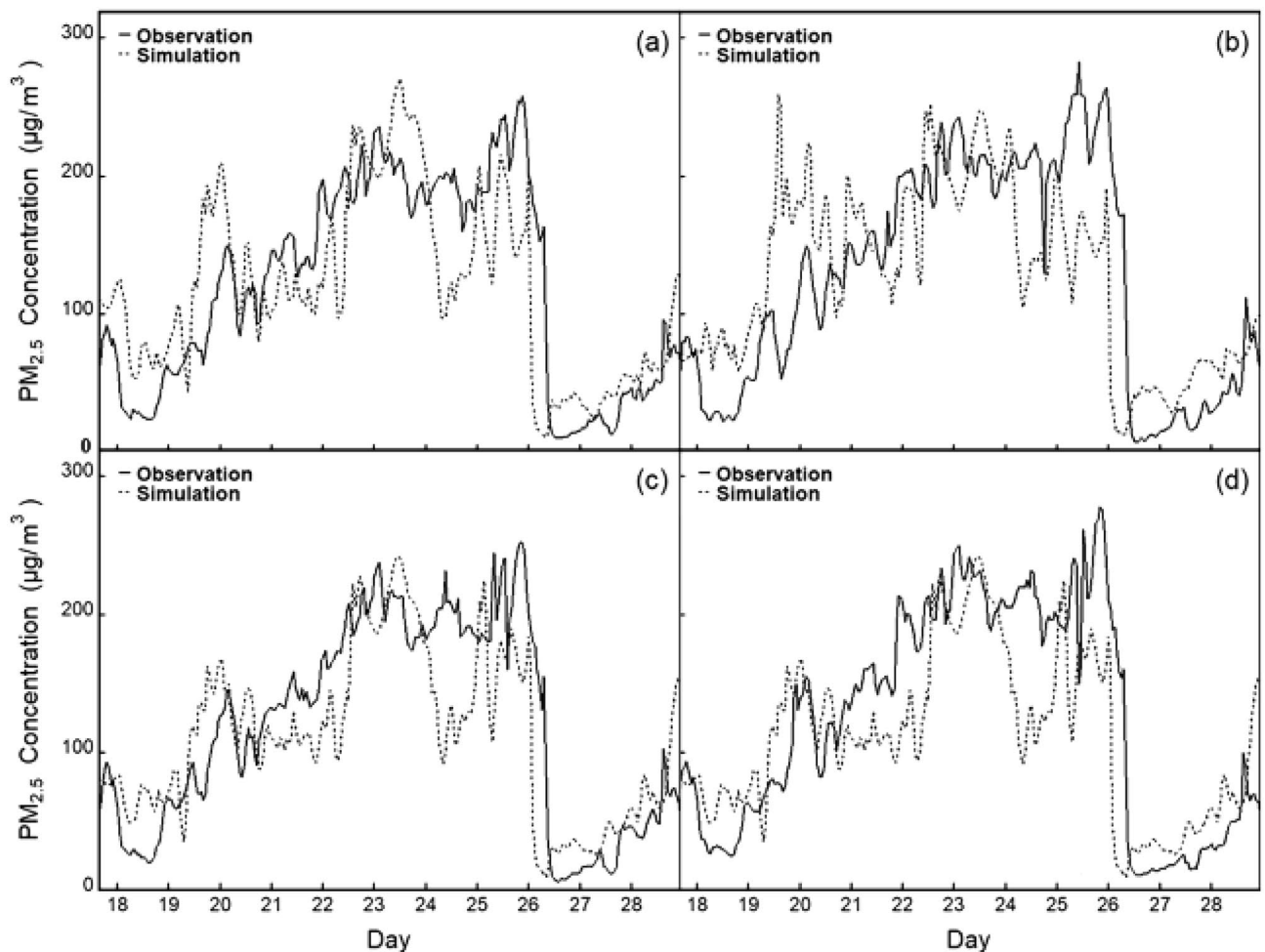


Figure 2. Hourly variations in observed (solid lines) and simulated (dashed lines) $PM_{2.5}$ concentrations at four monitoring sites in Zhengzhou during December 18–29, 2020. (a is the verification of observed and simulated values at 1316A station; b is the verification of observed and simulated values at 1319A station; c is the verification of observed and simulated values at 1320A station; d is the verification of observed and simulated values at 1324A station).

maximum simulated $PM_{2.5}$ concentration was obtained in the northwest area of Jiaozuo (Fig. 4a). This might have been related to the absence of obvious organized wind directions and weak wind speeds in this region. In most parts of Zhengzhou, the $PM_{2.5}$ concentrations exceeded $100 \mu\text{g m}^{-3}$, characterizing high- $PM_{2.5}$ -concentration environments. The lowest $PM_{2.5}$ concentration in Zhengzhou was over $80 \mu\text{g m}^{-3}$. In this area, the wind was strong, and the wind direction was mainly southward. High $PM_{2.5}$ concentrations were distributed in a band in this area. For PM_{10} , a similar spatial distribution was found; the highest PM_{10} concentration was found in the northwest area of Jiaozuo and was above $140 \mu\text{g m}^{-3}$, while Zhengzhou mostly had PM_{10} concentrations over $100 \mu\text{g m}^{-3}$. Zhengzhou and the area north of Zhengzhou were mainly affected by north winds. The high PM pollution concentrations identified in this area extended slightly from north to south.

Figure 5 shows the temporal variation in the simulated $PM_{2.5}$ concentration in Zhengzhou under S1. At 16:00 on December 20, the $PM_{2.5}$ concentrations were between 35 and $100 \mu\text{g m}^{-3}$ in most parts of Zhengzhou and its surrounding areas. At this time, the southeast wind speed reached 5 m s^{-1} . From 00:00 to 21:00 on December 21, pollutants accumulated in Zhengzhou with weak wind speeds. The highest $PM_{2.5}$ concentration was more than $120 \mu\text{g m}^{-3}$. At 16:00 on December 22, a slight increase appeared in the wind speed, and the wind turned southerly. The accumulated pollutants were blown away by winds. From 16:00 on December 20 to 16:00 on December 22, a high- $PM_{2.5}$ -concentration region was located north of Jiaozuo and Luoyang. At 08:00 on December 23, the $PM_{2.5}$ concentration in Zhengzhou was above $180 \mu\text{g m}^{-3}$ and even reached levels of $250 \mu\text{g m}^{-3}$ and above in northeastern Zhengzhou. The $PM_{2.5}$ concentrations were between 160 and $220 \mu\text{g m}^{-3}$ in the surrounding areas of Zhengzhou. At this moment, the northeast was the prevailing wind direction, and the wind speed was high. By 04:00 on December 24, the wind weakened, and the main wind direction became consistent with that recorded before. The heavily polluted area gradually moved southward. At 14:00 on December 24, however, the wind direction changed greatly and became an easterly wind. The pollutants in Xinxiang, Kaifeng, Xuchang and east of Zhengzhou were eradicated. The $PM_{2.5}$ concentrations dropped to below $75 \mu\text{g m}^{-3}$. At 04:00 on December 25, the wind weakened further, and the wind direction became disorganized. At 20:00 on December

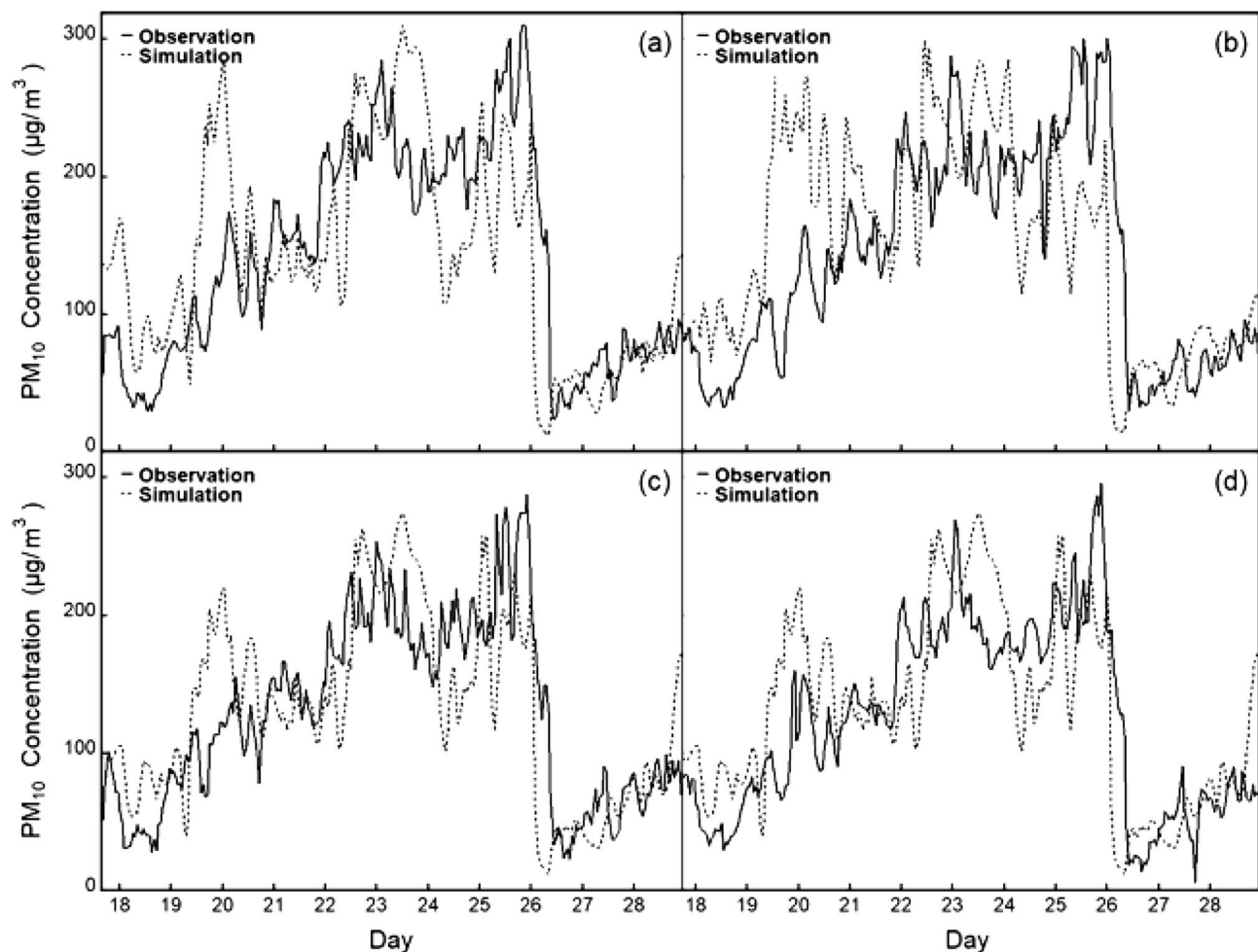


Figure 3. Hourly variations in observed (solid lines) and simulated (dashed lines) PM_{10} concentrations at four monitoring sites in Zhengzhou during the study period. (a) is the verification of observed and simulated values at 1316A station; (b) is the verification of observed and simulated values at 1319A station; (c) is the verification of observed and simulated values at 1320A station; (d) is the verification of observed and simulated values at 1324A station).

	Obs	Sim	MB	NMB	NME	RMSE	R
$PM_{2.5}$ ($\mu\text{g m}^{-3}$)	102.97	122.04	19.07	0.19	0.45	57.79	0.67
PM_{10} ($\mu\text{g m}^{-3}$)	119.10	148.47	29.36	0.25	0.47	71.76	0.55
DIR ($^{\circ}$)	165.37	159.22	-6.15	-0.04	0.30	95.19	0.67
SPD (m s^{-1})	4.44	3.66	-0.78	-0.18	0.49	2.71	0.38
TMP ($^{\circ}\text{C}$)	4.43	5.19	0.76	0.17	0.44	2.34	0.85
PRE (mm)	0.03	0	-0.03	-0.93	0.94	0.12	0.6

Table 3. Performance in meteorological conditions and PM concentrations of the WRF/Chem model in Zhengzhou.

25, the wind speeds in Xinxiang, Kaifeng, Xuchang and east of Zhengzhou increased, and the wind direction shifted to the northwest. $PM_{2.5}$ pollution started to spread rapidly to the east. At 06:00 on December 26, the main wind direction changed to a westerly wind, and the wind speed clearly increased in the northwest region. The high-pollution area moved eastward, and the $PM_{2.5}$ concentrations in Zhengzhou slightly decreased. At 12:00 on December 26, the wind speeds increased significantly, and the main wind direction remained northwest. The $PM_{2.5}$ concentration clearly decreased to below $120 \mu\text{g m}^{-3}$ in most areas.

Similar temporal variations in the simulated PM_{10} concentrations occurred in the simulated area (Fig. 6). At 16:00 on December 20, the spatial distribution of PM_{10} concentrations was similar to that of $PM_{2.5}$ concentrations. On December 21, the high- PM_{10} -concentration situation lasted all day. At 16:00 on December 22, an organized

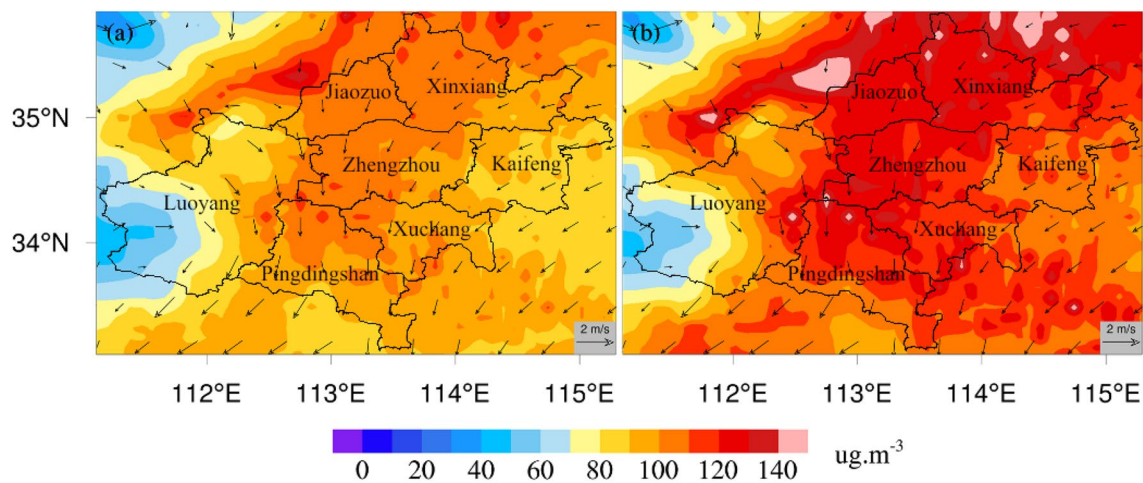


Figure 4. Spatial distributions of $PM_{2.5}$ (a) and PM_{10} (b) monthly mean concentrations in Zhengzhou.

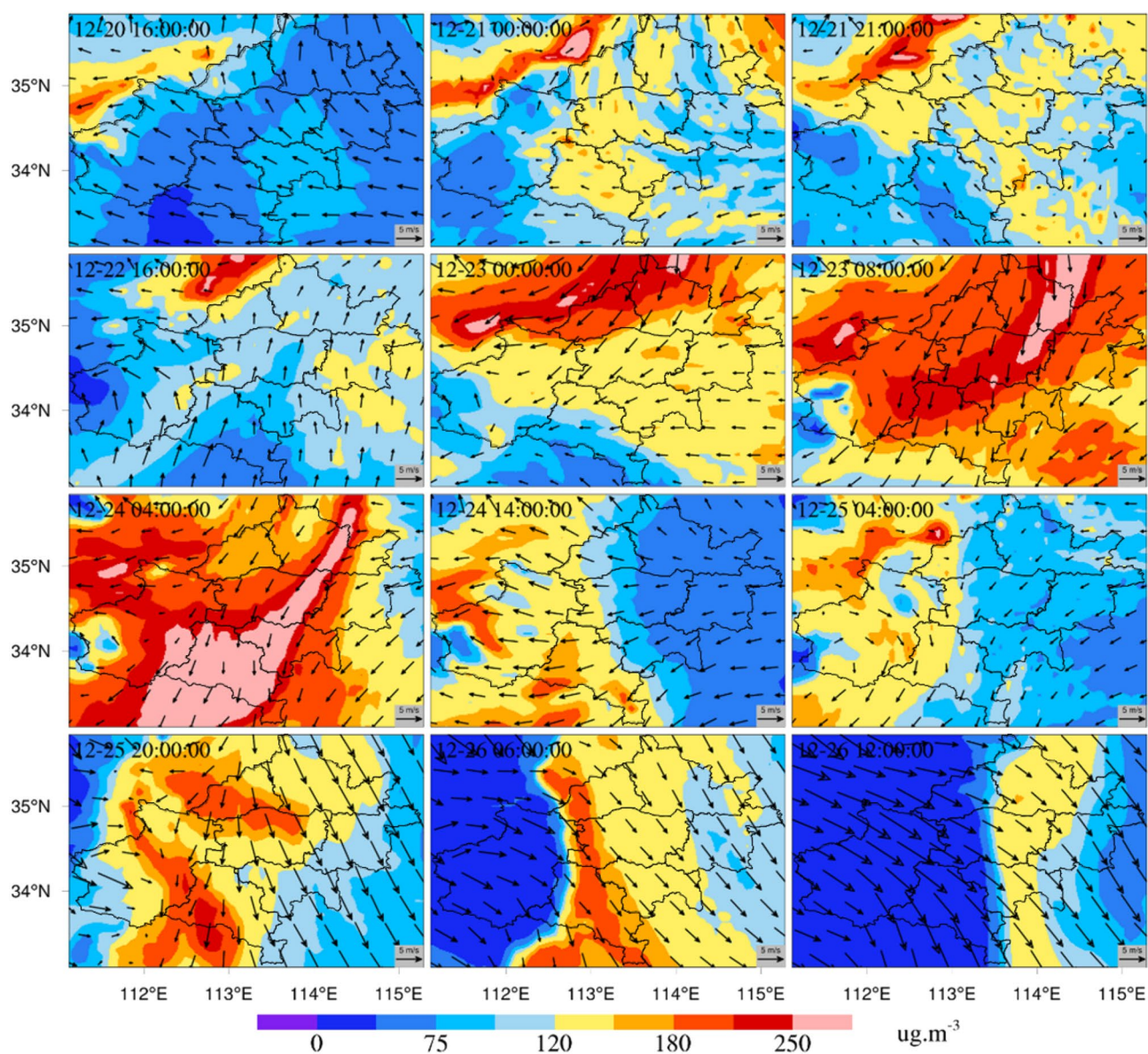


Figure 5. Spatial and temporal process of $PM_{2.5}$ concentrations in this pollution episode.

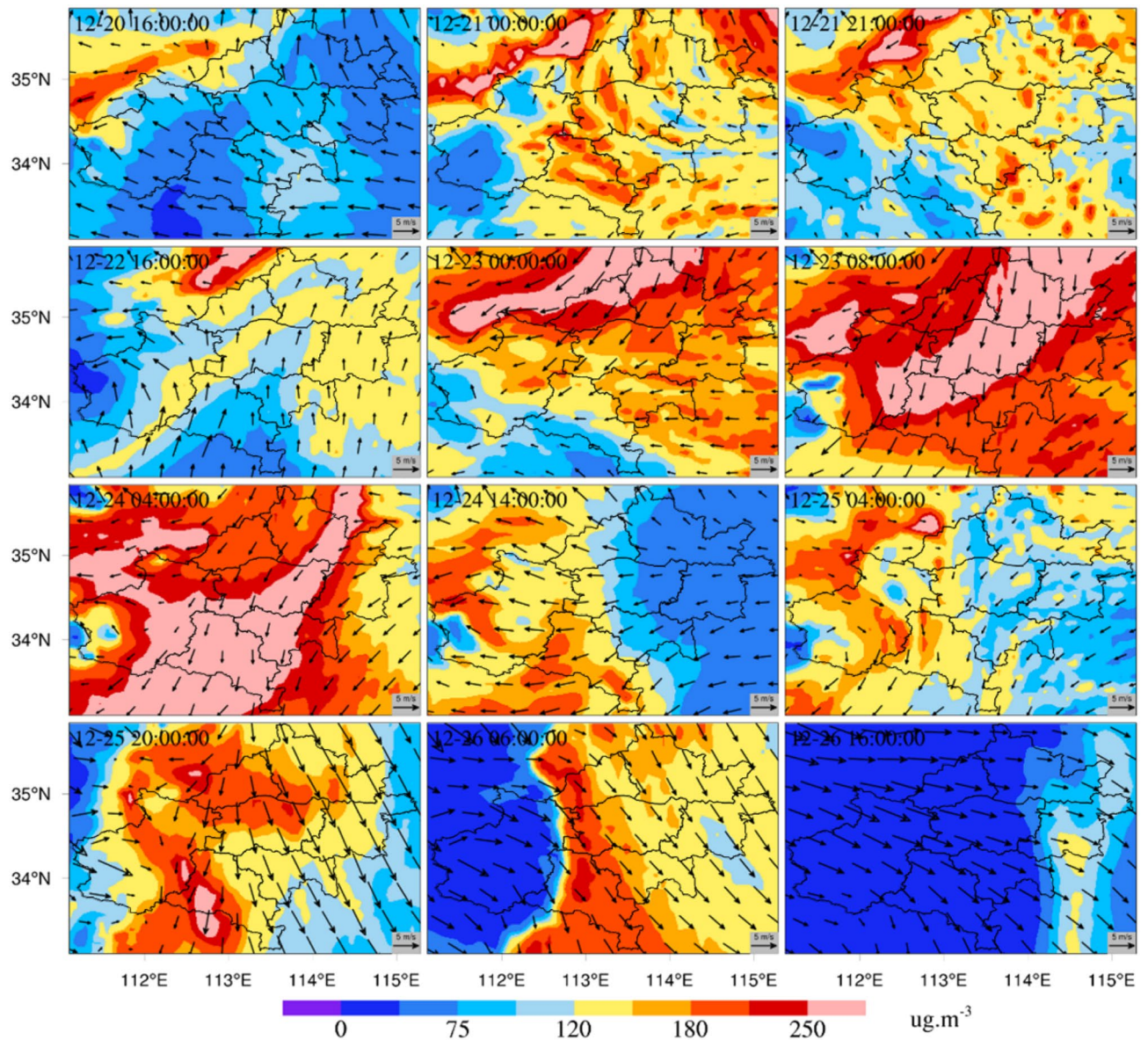


Figure 6. Spatial and temporal process of PM_{10} concentrations in this pollution episode.

wind direction emerged. Due to the south winds, the accumulated pollutant concentrations were reduced in Zhengzhou. At 00:00 on December 23, an obvious northerly wind could be identified north of Zhengzhou, and the high pollutant concentrations in this area spread to the south. At 08:00 on December 23, the PM_{10} concentrations were above $250 \mu\text{g m}^{-3}$ in Zhengzhou. The northeast winds caused high pollutant concentrations to continuously spread southward. At 04:00 on December 24, the high-pollutant-concentration area changed from impacting Zhengzhou and Xinxiang to spanning Luoyang, Pingdingshan and Xuchang. At 14:00 on December 24, the main wind direction became easterly, and high pollutant concentrations were thus transferred westward. Then, the wind conditions began to weaken and became disordered. At 04:00 on December 25, a slight PM_{10} accumulation occurred east of Zhengzhou. At 20:00 on December 25, the PM_{10} concentration was higher than that recorded hours earlier. At 06:00 on December 26, however, the winds in Zhengzhou and its surrounding areas were organized and developed into northwest winds with high speeds. Several hours of northwesterly winds caused the PM_{10} concentrations in Zhengzhou and its surrounding areas to significantly and rapidly decrease. At 16:00 on December 26, the PM_{10} concentrations were below $75 \mu\text{g m}^{-3}$ in most of Zhengzhou.

Trajectory analysis of the continuous heavy pollution process. In Fig. 7, the 72-h backward trajectories of the air mass arriving at Zhengzhou sampling point (1016A) at 00:00, 06:00, 12:00 and 18:00 every day were simulated for 9 consecutive days (December 19–27, 2019). The starting point of the simulated air mass was a height of 500 m above the Zhengzhou sampling point. On Dec. 19, this air mass was mainly a long-distance one from the north (Fig. 7a). On Dec. 20, the air mass was still dominated by long-distance air mass from the northwest (Fig. 7b). On Dec. 21, the air mass changed, the long-distance air mass from the northwest gradu-

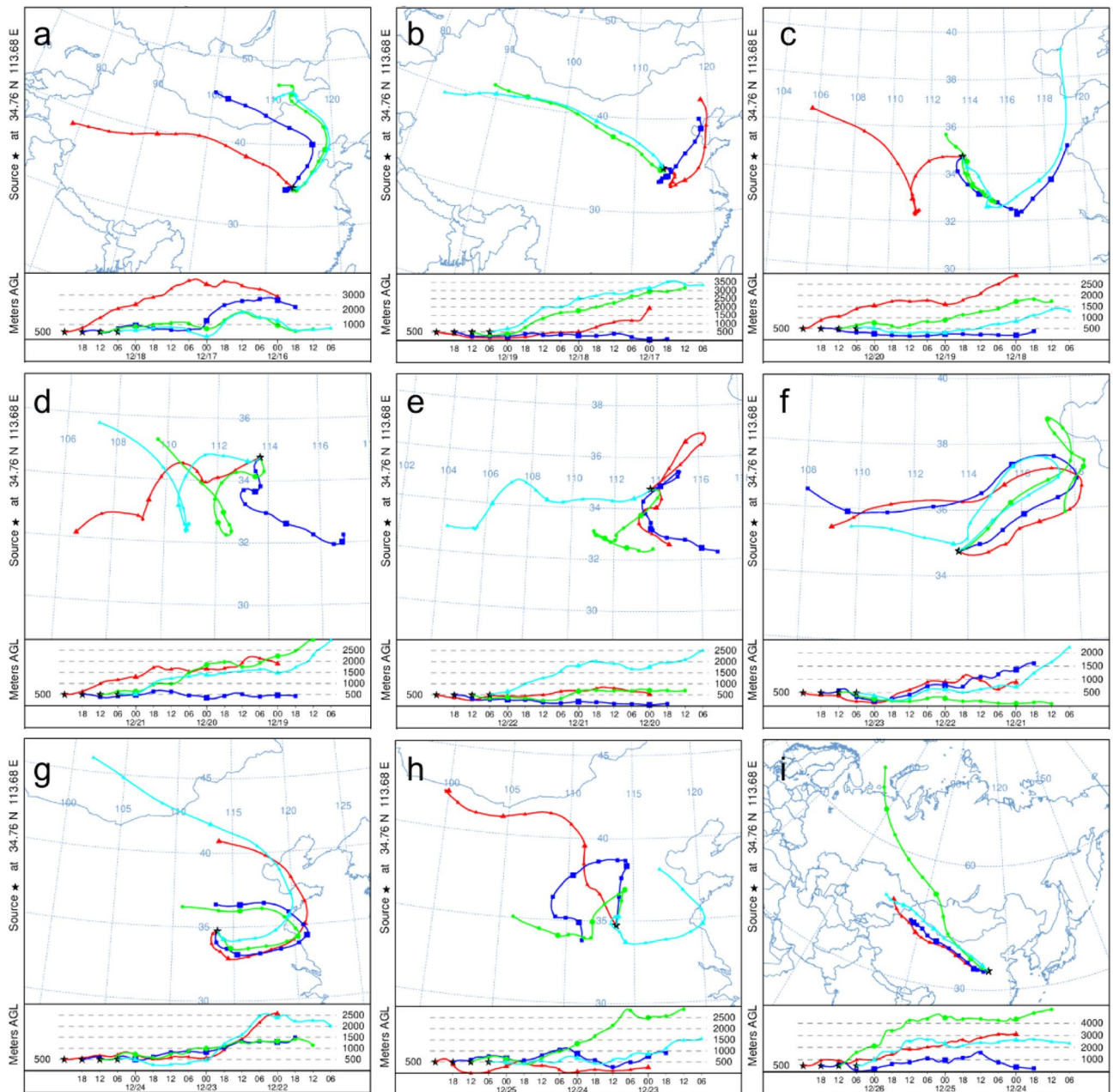


Figure 7. Backward trajectory from December 19 to 27, 2019 (**a–i** represent December 19, December 20, December 21, December 22, December 23, December 24, December 25, December 26 and December 27; the light blue track, green track, dark blue track, and red track indicate the air mass track arriving at 00:00, 06:00, 12:00 and 18:00, respectively).

ally disappeared, and the short-distance air mass from the east and southeast to Zhengzhou increased (Fig. 7c). On Dec. 22, the air mass changed again, as the air mass from the northeast disappeared. It comprised mainly a high-altitude air mass from the west (> 1500 m) and a small amount of low-altitude air mass from the southeast (< 500 m) (Fig. 7d). On Dec. 23, the air mass changed significantly, adding a short-range low-level air mass (< 1000 m) from the south and north, and the concentration of PM increased significantly (Figs. 5, 6, 7e). On Dec. 24, the low-altitude air mass from close range decreased, and the high-altitude air mass (> 1500 m) from the northwest increased. The PM concentration decreased (Figs. 5, 6, 7f). On Dec. 25, the long-distance high air mass (> 1500 m) from the north was the main air mass source, and the short-distance air mass source had a height of more than 1000 m (Fig. 7g). On Dec. 26, the low-level air mass (< 500 m) from the north began to enter, and the particulate concentration increased (Figs. 5, 6, 7h). On Dec. 27, a long-distance high air mass (> 2000 m) from the northwest became the primary source, and the particulate concentration at the observation station showed a significant downward trend (Fig. 7i). By analyzing the reverse trajectory of air mass, we found that in the heavy pollutant episode, an air mass less than 1000 m can cause PM to accumulate. The air mass

above 1000 m can reduce the PM concentration, so the inflow of a clean air mass at a high altitude can effectively alleviate the PM pollution.

Effects of local and surrounding emissions. There were different spatial distributions of the simulated mean $PM_{2.5}$ and PM_{10} concentrations under different schemes (Fig. 8). Decreased $PM_{2.5}$ and PM_{10} concentrations were observed in Zhengzhou and its surrounding areas under S2, S3, S4 and S5. Under scheme S2, the

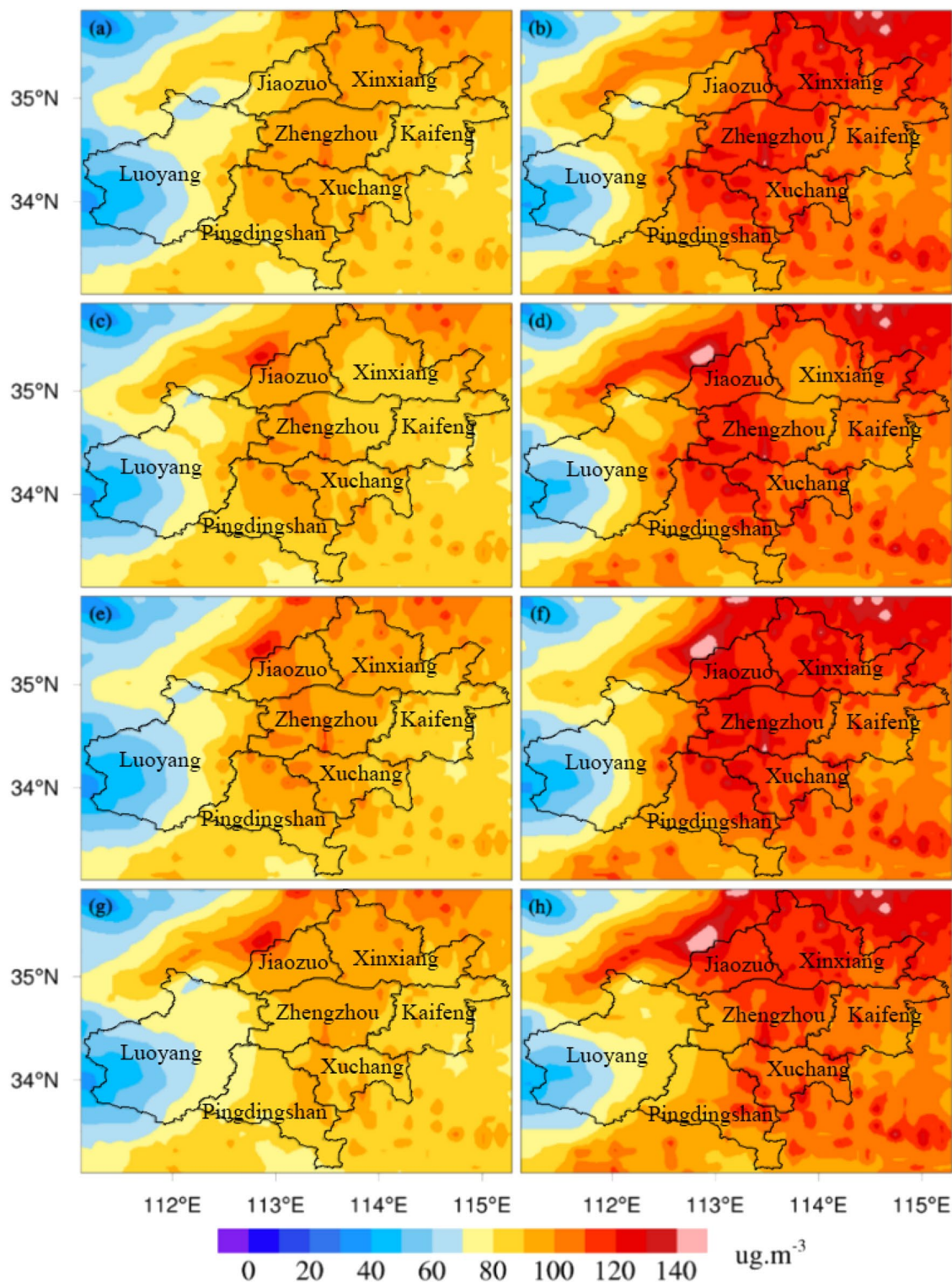


Figure 8. Spatial distributions of PM monthly mean concentrations under different scenarios ($PM_{2.5}$: a,c,e,g correspond to scenarios S2, S3, S4, and S5, respectively; PM_{10} : b,d,f,h correspond to scenarios S2, S3, S4, S5, respectively).

pollution sources in Zhengzhou were controlled. There was a significant drop in $PM_{2.5}$ concentrations in the region northwest of Zhengzhou (Fig. 8a). The mean simulated $PM_{2.5}$ concentration in Zhengzhou decreased by approximately $10 \mu\text{g m}^{-3}$. A similar decrease in PM_{10} concentrations in northwestern Zhengzhou can be seen in Fig. 8b. The emissions of Zhengzhou impacted the surrounding areas, and the largest impact occurred in the area to the northwest of Zhengzhou. Under scheme S3, the pollution sources in the area to the northeast of Zhengzhou (Xinxiang and Kaifeng) were controlled. The simulated $PM_{2.5}$ concentrations (Fig. 8c) were highest in the region to northwest of Zhengzhou but were slightly lower than those displayed in Fig. 4a. The $PM_{2.5}$ concentrations simulated at the junction of Zhengzhou, Xinxiang and Kaifeng were lower than those obtained in the base simulation. The pollution conditions in this area were more sensitive to the impact of emissions under scheme S3 than in other areas. The PM_{10} concentrations simulated under scheme S3 showed a similar change (Fig. 8d). Under scheme S4, the pollution sources in the area to the northwest of Zhengzhou (Luoyang and Jiaozuo) were controlled. The changes in the simulated spatial distributions of $PM_{2.5}$ and PM_{10} concentrations were the least obvious among the experiments comprising different schemes, and the pollutant concentrations decreased slightly (Fig. 8e,f). Under scheme S5, the pollution sources in the area to the south of Zhengzhou (Pingdingshan and Xuchang) were controlled. The simulated $PM_{2.5}$ and PM_{10} concentrations in regions to the south and southwest of Zhengzhou decreased significantly (Fig. 8g,h). The PM_{10} concentrations obviously decreased in western Zhengzhou. Among the four sensitivity experiments, the simulated change in the concentration of pollutants was the largest under scheme S5 compared to the case of scheme S1. Emissions from Zhengzhou significantly impacted the pollutant concentrations in the region to northwest of Zhengzhou. The impacts of emissions from Xinxiang and Kaifeng were obvious at the junction of Zhengzhou, Xinxiang and Kaifeng. In the area northwest of Zhengzhou, the impacts of local emissions were more obvious than those in other regions. Emissions from the southern region obviously impacted the southern and western areas of Zhengzhou.

Figure 9 shows the spatial distribution of the simulated values under the S1 scheme minus the simulated values under the control scenarios. As described in the previous section, the pollutant concentrations obviously decreased after removing local pollutant emissions from Zhengzhou (Fig. 9a,b). The area with the largest reduction in pollutant concentrations was located in the region northwest of Zhengzhou, with differences above $40 \mu\text{g m}^{-3}$. The concentration of pollutants changed dramatically in an area of northeastern Zhengzhou under S3 (Fig. 9c,d). The reductions in $PM_{2.5}$ concentrations were approximately $20 \mu\text{g m}^{-3}$, and the reductions in PM_{10} concentrations were even higher than $30 \mu\text{g m}^{-3}$ in northeastern Zhengzhou. The emissions from Xinxiang and Kaifeng had obvious impacts on the reduced pollutant concentrations in northeastern Zhengzhou. Under S5, the reductions in $PM_{2.5}$ and PM_{10} concentrations were approximately $40 \mu\text{g m}^{-3}$ at the junction of Zhengzhou, Luoyang and Pingdingshan. As in the other experimental schemes, the effect of emission-control measures on PM_{10} concentrations was greater than that on $PM_{2.5}$ concentrations. The experiments represented by S2 and S4 had little influence on reducing $PM_{2.5}$ and PM_{10} concentrations in Zhengzhou. In general, emissions from the pollution sources in Zhengzhou had a great impact on the particulate matter concentration in the area to the northwest of Zhengzhou. In addition, the emission of pollution sources in the area to the south of Zhengzhou had a more obvious impact on the area to the northwest of Zhengzhou.

The formula mentioned in section "Model settings" was used to calculate the contribution rates of emissions to air pollution concentrations in different regions. The local emissions of Zhengzhou had a certain contribution to its local pollutant concentrations, while the contribution to the central area of Zhengzhou was relatively weak (Fig. 10a,b). The contribution to the area to the northwest of Zhengzhou (the junction of Luoyang and Jiaozuo) peaked at more than 20%. The emissions from the area to the northeast of Zhengzhou strongly contributed to the $PM_{2.5}$ concentrations in the northeast area in Zhengzhou (Fig. 10c). The contribution to the PM_{10} concentrations in the northeast area in Zhengzhou was relatively strong, at more than 25% (Fig. 10d). The contribution to the $PM_{2.5}$ and PM_{10} concentrations were the highest in the northeast of Zhengzhou, gradually decreasing to the south, and the lowest in the downtown area. The emissions from the area to northeast Zhengzhou had an impact on northeast Zhengzhou, and the impact on the urban center was relatively limited. The emissions from the area to northwest of Zhengzhou had little influence on the local pollutant concentration in Zhengzhou (Fig. 10e,f). The contribution was approximately 5%. The contribution of the emissions from the area to northwest Zhengzhou to the center of Zhengzhou was negative. The contribution of these emissions to the junction of Luoyang and Jiyuan peaked at more than 30%. The emissions from the area to the south of Zhengzhou strongly impacted the local pollutant concentrations in Zhengzhou. The contribution of these emissions to the local pollutant concentration in Zhengzhou was above 5%, and this contribution was even above 25% southwest of Zhengzhou (Fig. 10g). The contribution distribution shown in Fig. 10h is similar to that shown in Fig. 10g; the contributions to PM_{10} concentrations in southwestern Zhengzhou were above 30%. The contribution of the emissions from the area to the south of Zhengzhou (Pingdingshan and Xuchang) to $PM_{2.5}$ and PM_{10} concentrations in Zhengzhou was larger than that in other areas (the area to the northeast and northwest of Zhengzhou). The contribution of these emissions to $PM_{2.5}$ and PM_{10} concentrations at the junction of Luoyang, Pingdingshan and Zhengzhou peaked at more than 35%.

The emissions from the region to the south of Zhengzhou (Pingdingshan and Xuchang) had the most serious impacts on the pollutant concentrations in Zhengzhou (Fig. 11). The contribution of the emissions from this area to the $PM_{2.5}$ concentrations in Zhengzhou was 14.39%. The contribution of the emissions from this area to the PM_{10} concentrations in Zhengzhou was 16.34%, 1.95% higher than that to the $PM_{2.5}$ concentrations. The emissions from the region to northwest Zhengzhou (Luoyang and Jiaozuo) had the weakest impact on pollutant concentrations in Zhengzhou. However, the contribution of the emissions from this area to PM_{10} concentrations (5.40%) was lower than that to $PM_{2.5}$ concentrations (5.96%). The emissions from the area to northeast of Zhengzhou (Xinxiang and Kaifeng) and the local area of Zhengzhou had similar impacts on the pollutant concentrations in Zhengzhou. The contributions of emissions from the area to the northeast of Zhengzhou and the local area of Zhengzhou to the PM_{10} concentrations in Zhengzhou were 7.18% and 7.29%, respectively. For

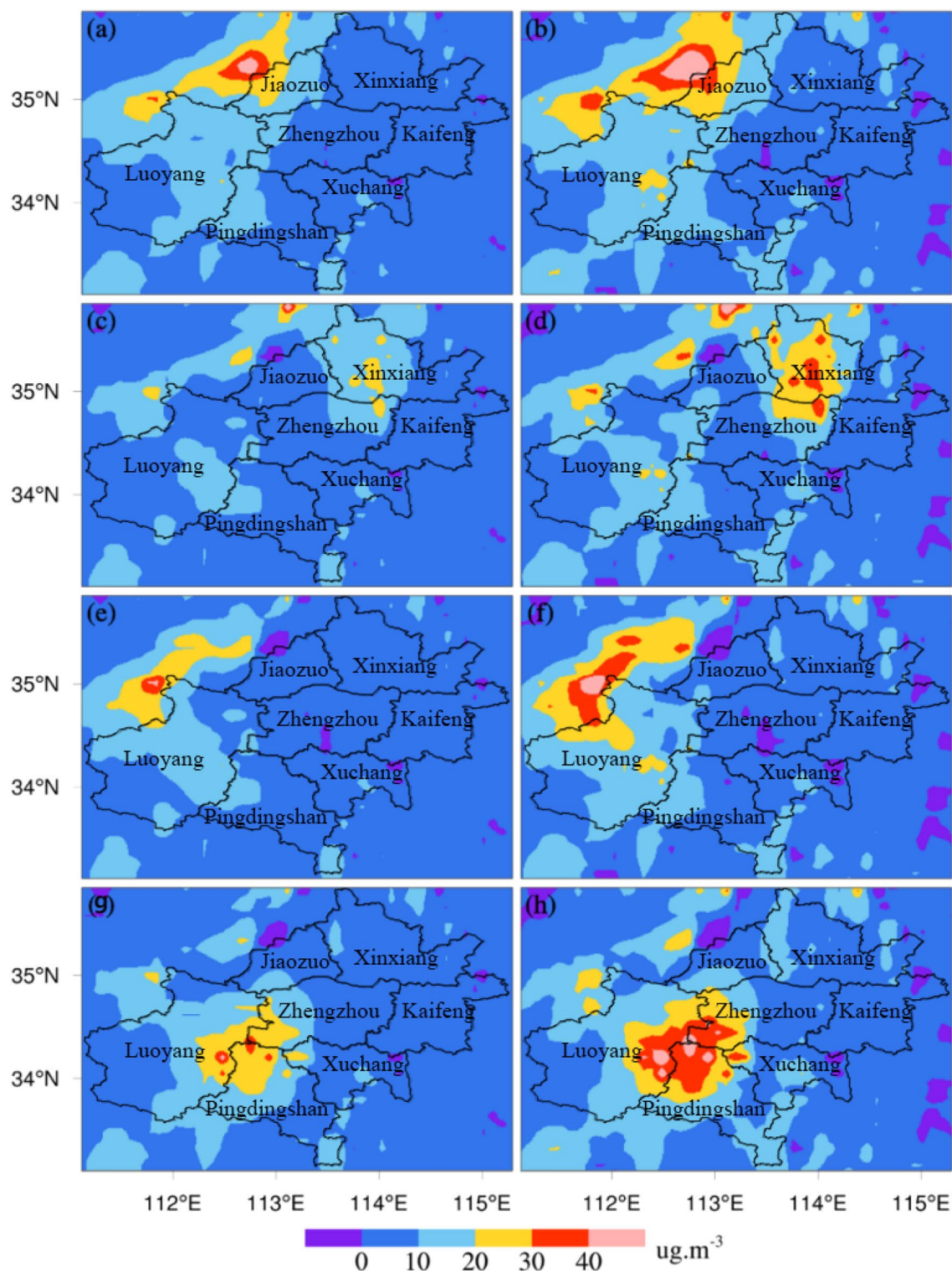


Figure 9. Spatial differences in PM concentrations between control scenarios (PM_{2.5}: a,c,e,g denote scenarios S2, S3, S4, and S5, respectively; PM₁₀: b,d,f,h denote scenarios S2, S3, S4, and S5, respectively).

the PM_{2.5} concentrations, the contributions of emissions from the area to the northeast of Zhengzhou and the local area of Zhengzhou were 7.42% and 7.94%, respectively.

Discussion

This study proved that the localized WRF/Chem model can effectively simulate regional-scale particulate pollution. The results show that by using the verification methods implemented in previous studies to verify the simulated peak concentrations of PM_{2.5} and PM₁₀ and the temporal variations in particulate concentration,

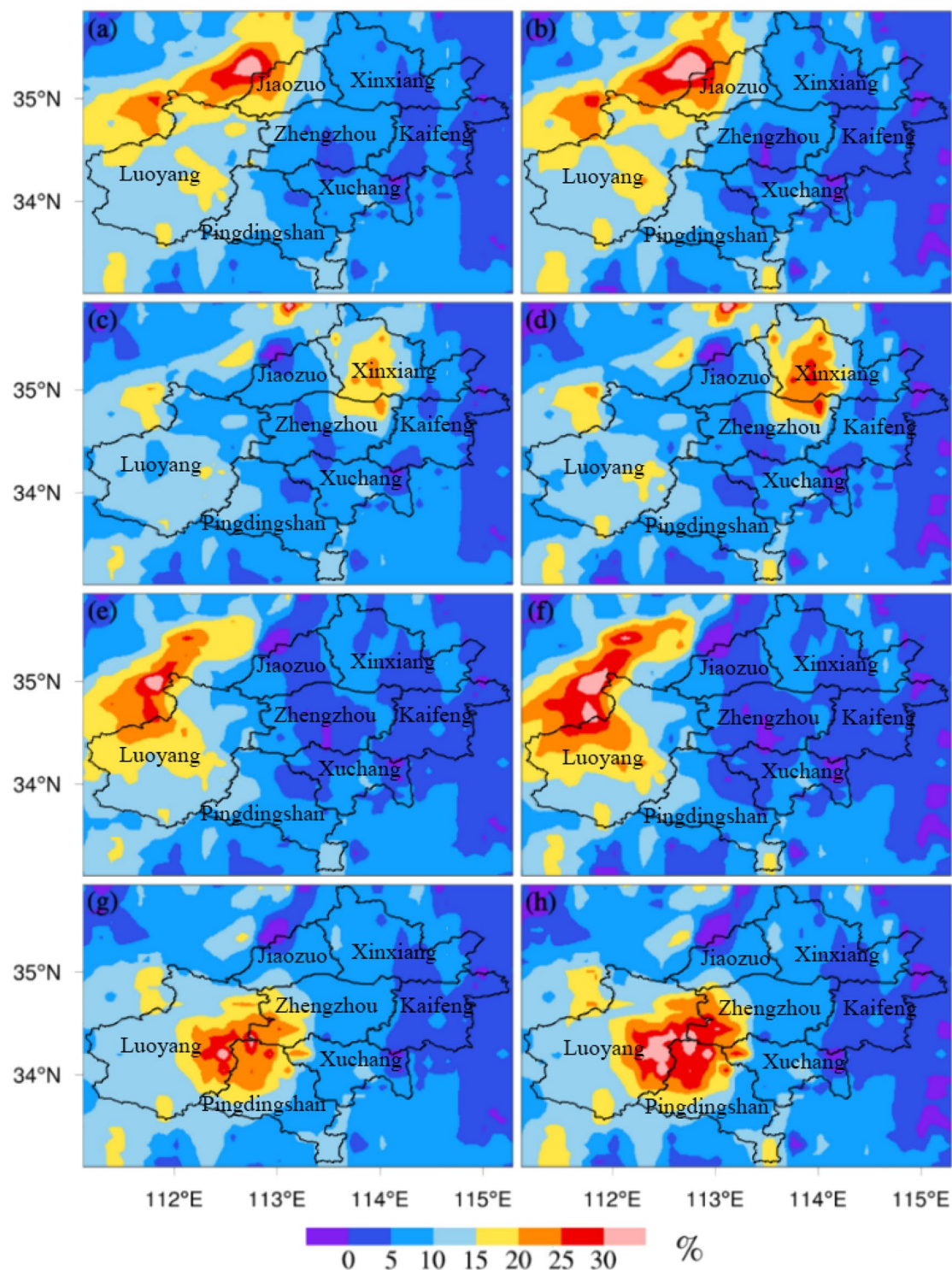


Figure 10. Spatial distributions of the contribution rates of different control scenarios to the PM concentrations in Zhengzhou ($PM_{2.5}$: a,c,e,g denote scenarios S2, S3, S4, and S5, respectively; PM_{10} : b,d,f,h denote scenarios S2, S3, S4, and S5, respectively).

wind speed, wind direction and temperature, the WRF/Chem model demonstrates high reliability for simulating particulate pollution temporal and spatial change patterns in Zhengzhou and its surrounding areas^{66,67}. The temporal and spatial sequence diagram of simulated and observed particulate concentrations from December 10–29, 2019, showed that the concentrations of $PM_{2.5}$ and PM_{10} calculated by WRF/Chem were consistent with the daily variation trend of observed data, indicating that WRF/Chem provides a relatively reasonable estimate

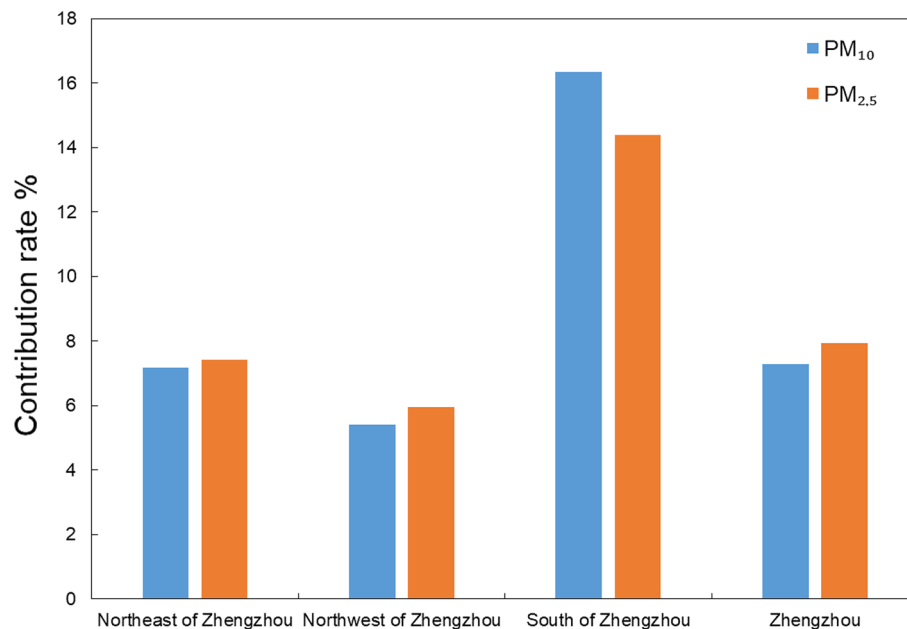


Figure 11. Contribution rate of anthropogenic emissions over surrounding areas to PM concentration in Zhengzhou.

for the emission of particulate pollution. Overall, the NMB and R values are within the range of previous research results^{68,69}.

The simulation results were highly similar to the particulate pollution pattern of Zhengzhou in winter simulated by Wang et al.⁷⁰ and Hu et al.⁷¹. During this period, northeast winds prevailed in Zhengzhou, which greatly promoted the transportation of particulate pollutants from northeast to south. The maximum simulated concentrations of PM_{2.5} and PM₁₀ in the Jiaozuo area were related to the lack of obvious organized wind direction and weak wind speed. Previous studies have proven that the pollution transmission process of particulate matter is greatly affected by meteorological factors. Wei et al. found that from October 8–11, 2014, the air quality in Beijing and Shijiazhuang continued to be heavily polluted over four days. On October 12, the weather situation changed, and systematic northerly winds developed in Northeast China, North China, Central China, East China and South China, with strong winds reaching 10 m/s in some parts, effectively removing pollutants. On the 12th, the air quality in Beijing, Shijiazhuang and other cities became excellent, and the continuous heavy pollution weather was effectively alleviated⁷². Strong wind is conducive to removing air pollutants in local areas and transporting air pollutants downwind⁶¹. The environmental conditions of continuous low wind speed are the main meteorological factors causing continuous pollution^{73,74}. To further study the regional particulate matter transport in Zhengzhou and its surrounding areas, we investigated the hourly variation in simulated concentrations of PM_{2.5} and PM₁₀ in Zhengzhou and its surrounding areas from December 20–26, 2019 (Figs. 5, 6). Driven by the northeast wind, the peak concentrations of surface PM_{2.5} and PM₁₀ pushed southward from Xinxiang and Jiaozuo to Zhengzhou. In the early morning of December 24, 2019, the peak concentration of particulate matter pushed southward from Zhengzhou to Pingdingshan and Xuchang, which showed that regional PM migration had a significant impact on PM pollution.

Based on the effective reproduction of the pollution characteristics of PM_{2.5} and PM₁₀ by the WRF/Chem model, sensitivity simulation experiments of different emission-control schemes were carried out to determine the impact of local and regional emissions on air quality in Zhengzhou. The simulation results under different emission-control schemes (Figs. 4, 7, 8) showed that in the four sensitivity tests, the change in simulated concentrations of PM_{2.5} and PM₁₀ under scheme S5 was the largest compared with scheme S1. The local pollution discharge in Zhengzhou had an impact on the particulate pollution in the surrounding areas. The greatest impact was in the area to the northwest of Zhengzhou, where the impact was more obvious than in other areas. The spatial distribution changes in PM_{2.5} and PM₁₀ concentrations simulated under scheme S4 were not significant in the tests with different schemes, and the emissions from the area to the northeast of Zhengzhou had no significant impact on any specific region. Emissions from the area to the south of Zhengzhou (Pingdingshan and Xuchang) significantly affected the southern and western regions of Zhengzhou.

According to the quantitative analysis of the simulation results, we found that the emissions from the area to south of Zhengzhou (Pingdingshan and Xuchang) had the most significant impact on the concentration of particulate pollutants in Zhengzhou. The contribution rate of emissions from this area to the PM_{2.5} concentration in Zhengzhou was 14.39%, and the contribution rate to the PM₁₀ concentration was 16.34%. The emissions from the area to northwest Zhengzhou (Luoyang and Jiaozuo) had the weakest impact on the pollutant concentration in Zhengzhou. The contribution rates of emissions to PM₁₀ and PM_{2.5} concentrations in this area were 5.40% and 5.96%, respectively. The surrounding areas contributed to the particulate pollution in Zhengzhou. According to the results, the contribution of local and surrounding emissions from pollution sources to the concentration

of particulate matter in Zhengzhou was in the following order: emissions of the area to the south of Zhengzhou were greater than emissions of the local area; emissions of the local area were greater than emissions of the area to northeast of Zhengzhou; emissions of the area to the northeast of Zhengzhou were greater than emissions of area to the northwest of Zhengzhou. The local emission of Zhengzhou was also an important contributor to the particulate pollution in Zhengzhou, but it was not the only source of the particulate pollution in Zhengzhou. Pollution transport from the surrounding areas was an important source of particulate pollution in Zhengzhou. In addition, the emissions of neighboring provinces (such as Shanxi, Shaanxi, Anhui and Shandong) were also important contributors to particulate pollution in Zhengzhou³³.

The objective of this study was to identify the contribution of anthropogenic emissions in different areas within Henan to the PM concentrations of Zhengzhou. Therefore, we mainly focused on quantifying the contribution of local and surrounding anthropogenic emissions to the PM concentration in Zhengzhou. However, this study did not simulate the contribution of different sectors (i.e., industry, transportation) to the PM concentration, which is important for proposing scientific emission reduction measures and also comprises the work that we will conduct next.

Conclusions

This study simulated the spatial and temporal variations in PM concentrations by using the WRF/Chem model and quantified its contribution rates from local and neighboring regions of Zhengzhou during a severe PM pollution episode. Emissions from the area to the south of Zhengzhou (Pingdingshan and Xuchang) were the most important contributors to particulate pollution in Zhengzhou among all the cities surrounding Zhengzhou during this episode. This region contributed 14.4% to the PM_{2.5} concentration and 16.3% to the PM₁₀ concentration in Zhengzhou. The local emissions and the emissions from the area to northeast Zhengzhou (Xinxiang and Kaifeng) had similar contributions to the PM_{2.5} (7.9% and 7.4%, respectively) and PM₁₀ (7.3% and 7.2%, respectively) concentrations in Zhengzhou. The emissions from the area to the northwest of Zhengzhou (Luoyang and Jiaozuo) had the weakest contribution. The contributions of the emissions from this area to the PM₁₀ and PM_{2.5} concentrations were 5.4% and 6.0%, respectively. We also found that the neighboring cities accounted for approximately 35% of the PM concentration in Zhengzhou, and approximately 2/3 of the contribution was transported from other regions, indicating that urban particulate pollution control to improve the urban air quality may be more effectively achieved by joint prevention and control in a wider area.

Data availability

The datasets generated during the current study are available from the corresponding authors on reasonable request.

Received: 3 October 2022; Accepted: 17 May 2023

Published online: 30 May 2023

References

- Zhang, Y. J., Cai, J., Wang, S. X., He, K. B. & Zheng, M. Review of receptor-based source apportionment research of fine particulate matter and its challenges in China. *Sci. Total Environ.* **586**, 917–929 (2017).
- Sahu, S. K. *et al.* Estimating ground level PM_{2.5} concentrations and associated health risk in India using satellite based AOD and WRF predicted meteorological parameters. *Chemosphere* **255**, 126969 (2020).
- Liu, X. M. *et al.* Effects of natural and anthropogenic factors and their interactions on dust events in Northern China. *CATENA*. **196**, 104919 (2021).
- Sharma, S., Sharma, R., Sahu, S. K. & Kota, S. H. Transboundary sources dominated PM_{2.5} in Thimphu, Bhutan. *Int. J. Environ. Sci.* **19**, 649–658 (2022).
- Li, X. Y. *et al.* Particulate matter pollution in Chinese cities: Areal-temporal variations and their relationships with meteorological conditions (2015–2017). *Environ. Pollut.* **246**, 11–18 (2019).
- Chen, H., Lin, Y., Su, Q. & Cheng, L. Q. Spatial variation of multiple air pollutants and their potential contributions to all-cause, respiratory, and cardiovascular mortality across China in 2015–2016. *Atmos. Environ.* **168**, 23–35 (2017).
- Zhang, Q. *et al.* Transboundary health impacts of transported global air pollution and international trade. *Nature* **543**(7647), 705 (2017).
- Deng, Q. H., Deng, L. J., Miao, Y. F., Guo, X. L. & Li, Y. G. Particle deposition in the human lung: Health implications of particulate matter from different sources. *Environ. Res.* **169**, 237–245 (2019).
- Schraufnagel, D. E. *et al.* Air pollution and noncommunicable diseases a review by the forum of international respiratory societies' environmental committee, part 2: Air pollution and organ systems. *Chest* **155**(2), 417–426 (2019).
- Zheng, G. J. *et al.* Exploring the severe winter haze in Beijing, the impact of synoptic weather, regional transport and heterogeneous reactions. *Atmos. Chem. Phys.* **15**(6), 2969–2983 (2015).
- Duan, K. *et al.* Impact of air pollution induced climate change on water availability and ecosystem productivity in the conterminous United States. *Clim. Change*. **140**(2), 259–272 (2017).
- Cheng, J. *et al.* Dominant role of emission reduction in PM_{2.5} air quality improvement in Beijing during 2013–2017: A model-based decomposition analysis. *Atmos. Chem. Phys.* **19**(9), 6125–6146 (2019).
- Reddington, C. L. *et al.* Exploring the impacts of anthropogenic emission sectors on PM_{2.5} and human health in South and East Asia. *Atmos. Chem. Phys.* **19**(18), 11887–11910 (2019).
- Wang, J. K., Zhang, H. D., Gui, H. L., Rao, X. Q. & Zhang, B. H. Relationship between atmospheric visibility and PM_{2.5} concentrations and distributions. *Huan Jing Ke Xue*. **40**(7), 2985–2993 (2019).
- Wang, H., Zheng, Q. P., Jiang, D. S. & Liao, K. Analysis of the variation characteristics of the total solar radiation and its relation with PM and O₃ in Fuzhou. *Ecol. Environ. Sci.* **29**(4), 771–777 (2020).
- Hu, J. L., Wang, Y. G., Ying, Q. & Zhang, H. L. Spatial and temporal variability of PM_{2.5} and PM₁₀ over the North China Plain and the Yangtze River Delta. *China. Atmos. Environ.* **95**, 598–609 (2014).
- Wang, L. T. *et al.* Application of Weather Research and Forecasting Model with Chemistry (WRF/Chem) over northern China: Sensitivity study, comparative evaluation, and policy implications. *Atmos. Environ.* **124**, 337–350 (2016).

18. Yang, X. C., Zhao, W. J., Xiong, Q. L., Wang, L. L. & Zhao, W. H. Spatio-temporal distribution of PM_{2.5} in Beijing-Tianjin-Hebei (BTH) area in 2016 and its relationship with meteorological factors. *Ecol. Environ. Sci.* **26**(10), 1747–1754 (2017).
19. Liu, Y. Z. *et al.* Dominant synoptic patterns and their relationships with PM_{2.5} pollution in winter over the Beijing-Tianjin-Hebei and Yangtze River Delta regions in China. *J. Meteorol. Res.-prc.* **33**(4), 765–776 (2019).
20. Dao, X. *et al.* Composition and sources of particulate matter in the Beijing-Tianjin-Hebei region and its surrounding areas during the heating season. *Chemosphere.* **13**, 2779 (2021).
21. Yin, X. H. *et al.* Source contributions to PM_{2.5} in Guangdong province, China by numerical modeling, results and implications. *Atmos. Res.* **186**, 63–71 (2017).
22. Cheng, N. N. *et al.* An integrated chemical mass balance and source emission inventory model for the source apportionment of PM_{2.5} in typical coastal areas. *J. Environ. Sci.* **92**, 118–128 (2020).
23. Luo, G. *et al.* Chemical composition and source apportionment of fine particulate matter in Xianlin area of Nanjing basing on-line measurement. *China Environ. Sci.* **40**(5), 1857–1868 (2020).
24. Wei, Z. *et al.* Source apportionment of PM_{2.5} in Handan City using a combined method of WRF/Chem and PMF model. *Environ. Sci. Technol.* **40**(11), 67–74 (2017).
25. Hu, Q. H. Characteristics and causes of typical pollution process in winter and spring in Fuzhou area. *Environ. Monit. China* **36**(3), 49–58 (2020).
26. Hu, Y. N., Ma, X. Y., Sha, T. & Gao, S. Impact of different emission sources on PM_{2.5} over East China based on numerical study. *China Environ. Sci.* **38**(5), 1616–1628 (2018).
27. Pan, Y. Z. *et al.* Source and sectoral contribution analysis of PM_{2.5} based on efficient response surface modeling technique over Pearl River Delta region of China. *Sci. Total. Environ.* **737**, 139655 (2020).
28. Li, Z. F. *et al.* Source contribution analysis of PM_{2.5} using response surface model and particulate source apportionment technology over the PRD region China. *Sci. Total. Environ.* **15**, 1757 (2021).
29. Jain, S. *et al.* Chemical characterization, source apportionment and transport pathways of PM_{2.5} and PM₁₀ over Indo Gangetic Plain of India. *Urban. Clim.* **36**, 100805 (2021).
30. Hopke, P. K. Review of receptor modeling methods for source apportionment. *J. Air. Waste. Manage.* **66**(3), 237–259 (2016).
31. Kumar, A., Jimenez, R., Belalcazar, L. C. & Rojas, N. Y. Application of WRF-Chem model to simulate PM₁₀ concentration over Bogota. *Aerosol. Air. Qual. Res.* **16**(5), 1206–1221 (2016).
32. Chen, D. S. *et al.* Estimating the contribution of regional transport to PM_{2.5} air pollution in a rural area on the North China Plain. *Sci. Total. Environ.* **583**, 280–291 (2017).
33. Liu, S. H. *et al.* Spatial-temporal variation characteristics of air pollution in Henan of China: Localized emission inventory, WRF/Chem simulations and potential source contribution analysis. *Sci. Total. Environ.* **624**, 396–406 (2018).
34. Chang, X. *et al.* Contributions of inter-city and regional transport to PM_{2.5} concentrations in the Beijing-Tianjin-Hebei region and its implications on regional joint air pollution control. *Sci. Total. Environ.* **660**, 1191–1200 (2019).
35. Dimitriou, K., Grivas, G., Liakakou, E., Gerasopoulos, E. & Mihalopoulos, N. Assessing the contribution of regional sources to urban air pollution by applying 3D-PSCF modeling. *Atmos. Res.* **248**, 105187 (2021).
36. He, J. J. *et al.* Source apportionment of particulate matter based on numerical simulation during a severe pollution period in Tangshan, North China. *Environ. Pollut.* **266**(3), 115133 (2020).
37. Cui, H. Y. *et al.* Source apportionment of PM_{2.5} in Guangzhou combining observation data analysis and chemical transport model simulation. *Atmos. Environ.* **116**, 262–271 (2015).
38. Huang, Y. Q. *et al.* Numerical simulations for the sources apportionment and control strategies of PM_{2.5} over Pearl River Delta, China, part I: Inventory and PM_{2.5} sources apportionment. *Sci. Total. Environ.* **634**, 1631–1644 (2018).
39. King, L. *et al.* Estimating organic aerosol emissions from cooking in winter over the Pearl River Delta region China. *Environ. Pollut.* **292**, 118266 (2022).
40. Li, N. *et al.* WRF-Chem modeling of particulate matter in the Yangtze River Delta region: Source apportionment and its sensitivity to emission changes. *PLoS ONE* **13**(12), e0208944 (2018).
41. Wu, X. R. *et al.* Comparative research on visibility and light extinction of PM_{2.5} components during 2014–17 in the North China plain 2014–2017. *Atmos. Ocean. Sci. Lett.* **14**(2), 100034 (2021).
42. Li, X. *et al.* Local and transboundary transport contributions to the wintertime particulate pollution in the Guanzhong Basin (GZB), China: A case study. *Sci. Total. Environ.* **797**, 148876 (2021).
43. Yang, J. H. *et al.* A hybrid method for PM_{2.5} source apportionment through WRF-Chem simulations and an assessment of emission-reduction measures in western China. *Atmos. Res.* **236**, 104787 (2020).
44. Zhang, Y. L. *et al.* The source apportionment of primary PM_{2.5} in an aerosol pollution event over Beijing-Tianjin-Hebei region using WRF-Chem. *China. Aerosol. Air. Qual. Res.* **17**(12), 2966–2980 (2017).
45. Wang, L. T. *et al.* Source apportionment of PM_{2.5} in top polluted cities in Hebei, China using the CMAQ model. *Atmos. Environ.* **122**, 723–736 (2015).
46. Yang, L. M. *et al.* Characteristics and formation mechanisms of secondary inorganic ions in PM_{2.5} during winter in a central city of China, Based on a high time resolution data. *Atmos. Res.* **233**, 104696 (2020).
47. Wu, J. *et al.* The moving of high emission for biomass burning in China, View from multi-year emission estimation and human-driven forces. *Environ. Int.* **142**, 105812 (2020).
48. Jiang, N. *et al.* Characteristics of mass concentration, chemical composition, source apportionment of PM_{2.5} and PM₁₀ and health risk assessment in the emerging megacity in China. *Atmos. Pollut. Res.* **9**(2), 309–321 (2018).
49. Liu, X. H. *et al.* Chemical characteristics, sources apportionment, and risk assessment of PM_{2.5} in different functional areas of an emerging megacity in China. *Aerosol. Air. Qual. Res.* **19**(10), 2222–2238 (2019).
50. Liu, X. H. *et al.* Composition analysis of PM_{2.5} at multiple sites in Zhengzhou, China: Implications for characterization and source apportionment at different pollution levels. *Environ. Sci. Pollut. R.* **28**(42), 59329–59344 (2021).
51. Tie, X. X., Geng, F. H., Li, P., Wei, G. & Zhao, C. S. Measurement and modeling of O₃ variability in Shanghai, China: Application of the WRF-Chem model. *Atmos. Environ.* **43**, 4289–4302 (2009).
52. Song, H. Q., Wang, K., Zhang, Y., Hong, C. P. & Zhou, S. H. Simulation and evaluation of dust emissions with WRF-Chem (v3.7.1) and its relationship to the changing climate over East Asia from 1980 to 2015. *Atmos. Environ.* **167**, 511–522 (2017).
53. Jiang, F. *et al.* Regional modeling of secondary organic aerosol over China using WRF-Chem. *J. Aerosol. Sci.* **43**(1), 57–73 (2012).
54. Grell, G. A. *et al.* Fully coupled “online” chemistry within the WRF model. *Atmos. Environ.* **39**(37), 6957–6975 (2005).
55. Tie, X. X. *et al.* Characterizations of chemical oxidants in Mexico City: A regional chemical/dynamical model (WRF-Chem) study. *Atmos. Environ.* **41**(9), 1989–2008 (2007).
56. He, H. *et al.* Analysis of the causes of heavy aerosol pollution in Beijing, China: A case study with the WRF-Chem model. *Particuology* **20**, 32–40 (2015).
57. Iraj, F., Memarian, M. H., Joghataei, M. & Malamiri, H. R. G. Determining the source of dust storms with use of coupling WRF and HYSPLIT models: A case study of Yazd province in central desert of Iran. *Dyn. Atmos. Oceans* **93**, 101–197 (2021).
58. Lin, Y., Farley, R. & Orville, H. Bulk parameterization of the snow field in a cloud model. *J. Appl. Meteorol. Clim.* **22**, 1065–1092 (1983).
59. Zaveri, R. & Peters, L. A new lumped structure photochemical mechanism for large-scale applications. *J. Geophys. Res. Atmos.* **104**, 30387–30415 (1999).

60. Hu, J. L. *et al.* Ensemble prediction of air quality using the WRF/CMAQ model system for health effect studies in China. *Atmos. Chem. Phys.* **17**(21), 13103–13118 (2017).
61. Yang, Y. R. *et al.* Characteristics and formation mechanism of continuous hazes in China, a case study during the autumn of 2014 in the North China Plain. *Atmos. Chem. Phys.* **15**(14), 8165–8178 (2015).
62. Mai, J. H. *et al.* A modeling study of impact of emission control strategies on PM_{2.5} reductions in Zhongshan, China, using WRF-CMAQ. *Adv. Meteorol.* **583**, 6070 (2016).
63. Kim, H. C. *et al.* Regional contributions to particulate matter concentration in the Seoul metropolitan area, South Korea: Seasonal variation and sensitivity to meteorology and emissions inventory. *Atmos. Chem. Phys.* **17**(17), 10315–10332 (2017).
64. Li, J. L. *et al.* Evaluation of the WRF-CMAQ model performances on air quality in china with the impacts of the observation nudging on meteorology. *Aerosol. Air. Qual. Res.* **22**(4), 1 (2022).
65. George, K. G. *et al.* Evaluation of WRF-Chem model (v3.9.1.1) real-time air quality forecasts over the Eastern Mediterranean. *Geosci. Model. Dev.* **15**, 4129–4146 (2022).
66. Gupta, M. & Mohan, M. Assessment of contribution to PM₁₀ concentrations from long range transport of pollutants using WRF-Chem over a subtropical urban airshed. *Atmos. Pollut. Res.* **4**(4), 405–410 (2013).
67. Du, Q. Y. *et al.* Modeling diurnal variation of surface PM_{2.5} concentrations over East China with WRF-Chem: impacts from boundary-layer mixing and anthropogenic emission. *Atmos. Chem. Phys.* **20**(5), 2839–2863 (2020).
68. Zhang, H. *et al.* Development of a source oriented version of the WRF-Chem model and its application to the California regional PM₁₀/PM_{2.5} air quality study. *Atmos. Chem. Phys.* **14**(1), 485–503 (2014).
69. Jat, R., Gurjar, B. R. & Lowe, D. Regional pollution loading in winter months over India using high resolution WRF-Chem simulation. *Atmos. Res.* **249**, 105326 (2021).
70. Wang, Q., Luo, K., Fan, J. R., Gao, X. & Cen, K. F. Spatial distribution and multiscale transport characteristics of PM_{2.5} in China. *Aerosol. Air. Qual. Res.* **19**(9), 1993–2007 (2019).
71. Hu, W. Y. *et al.* Importance of regional PM_{2.5} transport and precipitation washout in heavy air pollution in the Twain-Hu Basin over Central China: Observational analysis and WRF-Chem simulation. *Sci. Total. Environ.* **758**, 143710 (2021).
72. Wei, P. *et al.* Analysis of meteorological conditions and formation mechanisms of lasting heavy air pollution in eastern China in October 2014. *Res. Environ. Sci.* **28**(5), 676–683 (2015).
73. Hyde, P., Mahalov, A. & Li, J. L. Simulating the meteorology and PM₁₀ concentrations in Arizona dust storms using the weather research and forecasting model with chemistry (WRF-Chem). *J. Air. Waste. Manage.* **68**(3), 177–195 (2018).
74. Jiang, N., Duan, S. G., Yu, X., Zhang, R. Q. & Wang, K. Comparative major components and health risks of toxic elements and polycyclic aromatic hydrocarbons of PM_{2.5} in winter and summer in Zhengzhou: Based on three-year data. *Atmos. Res.* **213**, 173–184 (2018).

Acknowledgements

We the authors thank the Super Computing Center of Henan University, Kaifeng, China.

Author contributions

Conceptualization, G.S.; methodology, G.S.; software, Y.W., F.W., and R.M.; validation, Y.W., F.W., and R.M.; formal analysis, S.Z., H.Z., and X.R.; investigation, H.X.; resources, X.R.; data curation, H.Z. and X.R.; writing—original draft preparation, Y.W.; writing—review and editing, G.S., and S.Z.; visualization, F.W., Y.W., and H.X.; supervision, G.S.; project administration, G.S.; funding acquisition, G.S. All authors have read and agreed to the published version of the manuscript.

Funding

This research was funded by Training Plan for Young Backbone Teachers in Colleges and Universities in Henan Province, China, grant number 2021GGJS024 and the National Nature Science Foundation of China, grant number 41871316.

Competing interests

The authors declare no competing interests.

Additional information

Correspondence and requests for materials should be addressed to G.S. or H.S.

Reprints and permissions information is available at www.nature.com/reprints.

Publisher's note Springer Nature remains neutral with regard to jurisdictional claims in published maps and institutional affiliations.



Open Access This article is licensed under a Creative Commons Attribution 4.0 International License, which permits use, sharing, adaptation, distribution and reproduction in any medium or format, as long as you give appropriate credit to the original author(s) and the source, provide a link to the Creative Commons licence, and indicate if changes were made. The images or other third party material in this article are included in the article's Creative Commons licence, unless indicated otherwise in a credit line to the material. If material is not included in the article's Creative Commons licence and your intended use is not permitted by statutory regulation or exceeds the permitted use, you will need to obtain permission directly from the copyright holder. To view a copy of this licence, visit <http://creativecommons.org/licenses/by/4.0/>.

© The Author(s) 2023